Recent advances in numerical and experimental downwind sail aerodynamics

Journal of Sailing Technology 2019, volume 4, issue 1, pp. 45 - 65.
The Society of Naval Architects and Marine Engineers.

Recent Advances in Numerical and Experimental Downwind Sail Aerodynamics

Jean-Baptiste R. G. Souppez
Warsash School of Maritime Science and Engineering, Solent University, UK.

Abel Arredondo-Galeana
School of Engineering, Institute for Energy Systems, University of Edinburgh, Edinburgh, UK.

Ignazio Maria Viola
School of Engineering, Institute for Energy Systems, University of Edinburgh, Edinburgh, UK, i.m.viola@ed.ac.uk.

Manuscript received June 22, 2019; accepted as submitted, September 11, 2019.

Abstract. Over the past two decades, the numerical and experimental progresses made in the field of downwind sail aerodynamics have contributed to a new understanding of their behaviour and improved designs. Contemporary advances include the numerical and experimental evidence of the leading-edge vortex, as well as greater correlation between model and full-scale testing. Nevertheless, much remains to be understood on the aerodynamics of downwind sails and their flow structures. In this paper, a detailed review of the different flow features of downwind sails, including the effect of separation bubbles and leading-edge vortices will be discussed. New experimental measurements of the flow field around a highly cambered thin circular arc geometry, representative of a bi-dimensional section of a spinnaker, will also be presented here for the first time. These results allow interpretation of some inconsistent data from past experiments and simulations, and to provide guidance for future model testing and sail design.

Keywords: Downwind Yacht Sails; Spinnakers; Circular Arc; Aerodynamics, Racing Yachts.

NOMENCLATURE

AoA	Angle of Attack
CFD	Computational Fluid Dynamics
DES	Detached Eddy Simulation
FEA	Finite Element Analysis
FSI	Fluid-Structure Interaction
LE	Leading-Edge
LES	Large Eddy Simulation
LEV	Leading-Edge Vortex
LSB	Laminar-Separation Bubble
NACA	National Advisory Committee for Aeronautics
PIV	Particle Image Velocimetry
RANS	Reynolds-Averaged Navier Stokes
Re	Reynolds Number
TKE	Turbulent Kinetic Energy
VLM	Vortex Lattice Method

1. INTRODUCTION

Sailing has been a central part of history, and has heavily influenced the development of humanity, with evidence of sailing vessels as early as the 6th millennium BC (Carter, 2006). While sailing downwind has benefited from millennia of evolution, the very first instance of a highly cambered and dedicated downwind sail, termed spinnaker, did not occur until 1865, as reported by King (1981), and was not popularized until the 1970s and 1980s; primarily thanks to the development of symmetric spinnakers for the America's Cup.

Asymmetric spinnakers were then introduced in the 1980s in the 18ft fleet in Sydney, before being popularised on offshore racing yachts in the 1990s. These new sails were promptly adopted in many significant sailing events; firstly in offshore races such as the Vendée Globe and the Whitbread 60, and later in the America's Cup (Fallow, 1996; Richards et al., 2001; Viola & Flay, 2009). The significant advances made in terms of spinnaker design and analysis during this particular decade can be related to the greater part that downwind legs took in the 1995 America's Cup (Fallow, 1996), thus motivating further research and development.

The 1990s also coincide with a fast increase in accessible computational power, allowing advanced numerical methods to be used in sail design (Hedges, 1993; Hedges et al., 1996), particularly for downwind sails. Upwind sails, where the flow remains largely attached, have been successfully analysed using inviscid codes since the 1960s, with the pioneering work of Milgram (1968) on Vortex Lattice Method (VLM), and later Gentry (1971), to eventually be extensively utilized in America's Cup sails development (Gentry, 1988). Conversely, for downwind sails, where the flow is largely separated, the use of Reynolds-Averaged Navier-Stokes (RANS) simulations is necessary (Lasher et al., 2005). The first instances of RANS occurred in 1996 for downwind sails (Hedges et al., 1996) and 1999 for upwind sails (Miyata & Lee, 1999). The complexity of downwind sail flow also prompted the development of dedicated experimental facilities, namely twisted flow wind tunnels (Flay & Vuletich, 1995), the need for which was highlighted a few years before by Flay & Jackson (1992).

One of the benefits of experimental testing is the ease of achieving the effective flying shape of the sail from the moulded one. In order to achieve the flying shape from numerical simulations, Computational Fluid Dynamics (CFD) is coupled with Finite Element Analysis (FEA). This approach has led to major advances in the field of Fluid-Structure Interaction (FSI) of downwind sails (Richter et al., 2003; Renzsch et al., 2008; Durand, et al., 2014; Sacher et al., 2015).

With the continuous growth of computational power (Viola, 2009), leading in 2011 to over a billion cells being used for yacht sail simulations for the first time (Viola & Ponzini, 2011), and with the wide adoption of asymmetric spinnakers, there is more than ever a strong incentive to employ numerical methods to further the understanding of downwind sails design. This has recently enabled the discovery of the Leading-Edge Vortex (LEV). Indeed, the first evidence of the presence of a stable LEV on a downwind yacht sail was provided numerically in 2014 (Viola et al., 2014), before being confirmed experimentally three years later (Viola & Arredondo-Galeana, 2017; Arredondo-Galeana & Viola, 2018), prompting new interpretations of full-scale pressure measurements on downwind sails (Richards & Viola, 2015).

This paper first introduces the background to the LEV, and the numerical and experimental work demonstrating its presence and impact on sailing performance. Then, the correlation

between full-scale experiments, numerical simulations and model-scale testing are presented, focusing on recent findings and discrepancies. Successively, novel results are introduced to understand anomalies observed in pressure distributions between various experiments at model-scale. The findings of this experiment will be discussed, eventually concluding on the recent advances in downwind sail aerodynamics, and suggesting refined wind tunnel testing practices for future experimental work.

2. LEADING EDGE FLOW

The LEV identified on yacht sails has significant similarities with that on delta wings. Following the work undertaken by the National Advisory Committee for Aeronautics (NACA) during World War II, and driven by the will to achieve supersonic planes, a vast amount of research was undertaken on delta wings. The leading-edge separation highlighted in the 1950s (Marsden et al., 1958; Harvey, 1959) then resulted in the theory developed by Hall (1961) and applied by Earnshaw (1962) in the early 1960s. The LEV on delta wings (pictured in Figure 1a) provides most of the lift at high angles of attack (AoA). Anecdotally, Bethwaite (1993) anticipated that highly swept back asymmetric spinnakers could function in a similar fashion as delta wings on high performance dinghies. It was subsequently hypothesised by Viola & Flay (2012) that an LEV, analogous to that of delta wings, was present at the head of spinnakers on both the leading and trailing edges, provided that sailing occurs at sufficiently high apparent wind angles.

Vortex lift was modelled successfully by Polhamus (1966) for slender delta wings through the ‘suction force analogy’. Despite the LEV being inherently tri-dimensional, the contribution of the vortex to the sectional lift can be modelled as a 2D effect using this analogy, which is based on the leading-edge suction associated with potential-flow leading-edge singularity. Saffman & Sheffield (1977) further explored theoretically the effect of a ‘trapped’, two-dimensional vortex near the leading edge of a flat plate through inviscid potential flow. They found that at suitable locations the vortex might remain stationary relative to the flat plate and that the vortex provides a significant lift contribution. At the leading-edge, however, the vortex was sensitive to flow disturbances and no stable positions were found. Huang & Chow (1982) expanded the study to circular arcs and Joukowski airfoils and found consistent results.

More recently, a tri-dimensional LEV was found to be the reason for the Hawkmoth (manduca sexta), and more generally insects, being able to fly thanks to the lift contribution of the LEV. This pioneering work and flow visualization realized in 1996 (Ellington et al., 1996) was validated using Particle Image Velocimetry (PIV) in 2005 (Bomphrey et al., 2005). Around the same time, in 2004, evidence of LEV on bird wings was also provided (Figure 1b, Videler et al., 2004) suggesting lift enhancement. This seminal work on insect and bird flight led to significant studies of the LEV on oscillating and revolving wings (Figure 1c, Taira & Colonius, 2009) and has been of paramount importance to understand the different stabilization mechanisms that allow a vortex to remain stably (‘trapped’) near a wing (Eldredge & Jones, 2019). In the case of spinnakers (Figure 1d), the LEV has similarities with that of bird wings (Figure 1b) and translating wings (Figure 1c) due to the comparable sweepback angle and strong interaction with the tip vortex.

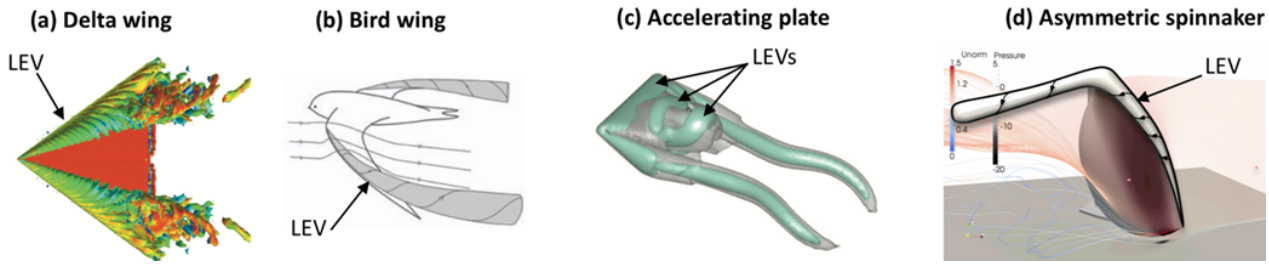

Figure 1: The LEV on different lifting surfaces. (a) The steady LEV of a delta wing (Mitchell et al., 2006); (b) the steady LEV on a gliding bird's wing (similar to the periodic LEV on flapping wings) (Videler et al., 2004); (c) the unsteady LEV of an accelerating plate after having convected 5 chord lengths (Taira & Colonius, 2009); and (d) the intermittently steady LEV on an asymmetric spinnaker.

It is to note that the LEV has been identified across a wide range of Reynolds numbers (Re). In laminar flow conditions, it has been found on auto-rotating seeds (Lentink et al., 2009) and on the wings of insects (Muijres et al., 2008) and small birds (Lentink et al., 2007). In transitional and turbulent flow conditions, it has been detected on larger bird wings (Hubel & Tropea, 2010), fish fins (Borazjani & Daghooghi, 2013) and delta wings (Gursul et al., 2005, Gursul et al., 2007).

In the examples above, the LEV provides an essential source of lift augmentation, also delaying stall. However, the LEV is not always desirable. In helicopter rotors (Corke et al., 2015) and wind turbines (Larsen et al., 2007) the LEV is a powerful but dangerous flow feature, since it generates large load oscillations. When the LEV is shed downstream, it leads to a lift overshoot above the quasi-static maximum lift, as well as an abrupt and dangerous change in the pitching moment.

A key characteristic of the LEV is that it is a feature of the instantaneous flow field, and not of the time-averaged one. This is relevant to yacht sails, where a distinction can be made between the recirculating flow at the leading edge of upwind sails, such as jibs and genoas, and that of downwind sails.

Time-averaged vortices include those on upwind sails, where the leading-edge bubble is similar to those of flat plates at incidence characterised by Newman & Tse (1992), and those of plates with a blunt leading edge (Figure 2a and 2b). Another time-averaged vortex is that occurring as a result of a detached boundary layer, giving a region of recirculating reverse flow (O'Meara & Muller, 1987). This type of bubbles typically occurs on thin foils and reattachment is due to the laminar-to-turbulent transition of the separated shear layer (Crabtree, 1957); in this case they are called Laminar-Separation Bubbles (LSB) (Figure 2c). Bubbles and their impact on the flow field and resulting pressure distribution was extensively discussed by Ward (1963), with the characteristic plateau in the pressure coefficient indicating the presence of a bubble. This will be emphasized in the following sections, when discussing the pressure distribution over asymmetric spinnakers.

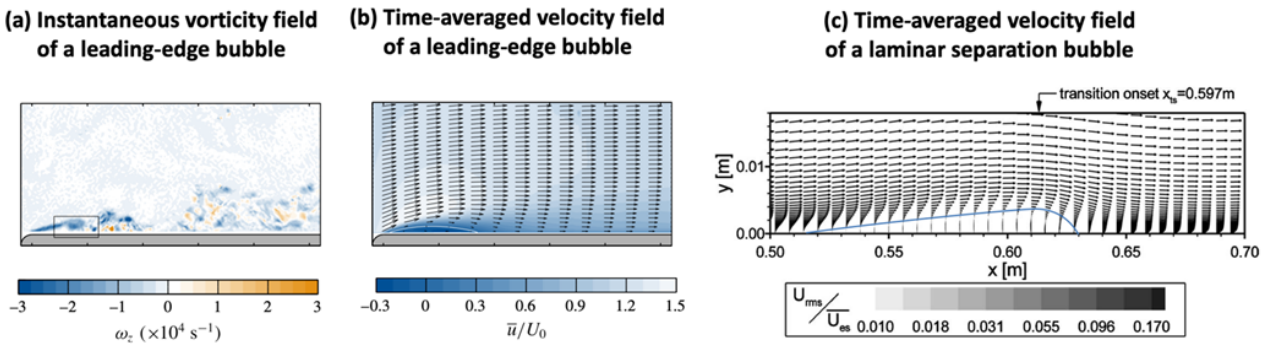

Figure 2: Leading-edge bubble and laminar-separation bubble. The vorticity (a) and velocity field (b) of a leading-edge bubble measured by Stevenson et al. (2016) and the velocity field of a laminar-separation bubble (c) measured by McAuliffe & Yaras (2010).

On the other hand, spinnakers generate a much more coherent vortex structure that can be identified in the instantaneous flow field. This vortex is formed by the roll of vorticity at the leading edge, as identified on, and exploited by both biological flyers and delta wings, with a significant increase in performance. The underlying stabilization mechanisms that allows the LEV to be more coherent on spinnakers than on upwind sails are still to be fully understood. Arredondo-Galeana (2019) suggested that the sweep back of the leading edge, and the strong tip vortex, are the main elements that improve the stability of the LEV on downwind sails. Finally, it is interesting to note that the interference of the mast on the mainsail results in two counter-rotating vortices on the windward and leeward side of the mast (Fossati, 2009; Larsson et al., 2013). The vortex lift due to these two coherent vortices is unlikely to cancel each other, and their net contribution has never been estimated.

3. THEORETICAL CONSIDERATIONS

The mechanism by which the LEV contributes to lift is as follow. Let assume that the sail is trimmed at the ideal angle of attack, i.e. that the flow velocity is tangent to the sail at the leading edge and no LEV occurs. The integral of the vorticity in the sail boundary layer is equal to the ‘bound’ circulation, which represents the strength of a vortex inside of the sail (‘bound to the sail’). The Kutta-Joukowski’s theorem states that the lift is proportional to the bound circulation. If the sail is trimmed at higher angles of attack, the sharp leading edge leads to flow separation. Without the LEV, the sail would stall and both circulation and lift would decrease. With the LEV, the loss in bound circulation is accounted for, at least in part, by unbound circulation which is contained within the LEV. Its circulation contributes to the lift of the sail to a different extent depending on its position and velocity (Li & Wu, 2018). Hence, the LEV retains some of the circulation that would otherwise be lost. In some cases, such as in Figure 3, it also enables flow reattachment. In these cases, the LEV is said to be ‘trapped’ by the streamlines that keep it attached to the sail. The sum of the bound circulation and the circulation in the trapped vortex is equal to the circulation that the sail would have if the boundary layer was attached without the presence of the vortex (DeVoria & Mohseni, 2017).

4. LEADING-EDGE VORTEX OF DOWNWIND SAILS: NUMERICAL SIMULATIONS

The use of Detached Eddy Simulation (DES) revealed the presence of an LEV on a model-scale sail. The vortex size was shown to increase spanwise towards the head of the sail. The visual representation of the numerical evidence of the LEV, related to the work of Viola

et al. (2014), is depicted in Figure 3. The LEV can be identified as the region of high vorticity, whose contour is shows by the isoline of vorticity. Remarkably, the isoline of axial velocity shows reveals that, inside the core of the LEV, the flow velocity u_a along the axis of the vortex (out of the plane of the figure) is even higher than the free stream velocity U. This region of very high velocity is associated with a low pressure, with a pressure coefficient ranging from -2 to -4. The time-averaged streamline shows the reattachment downstream of the LEV.

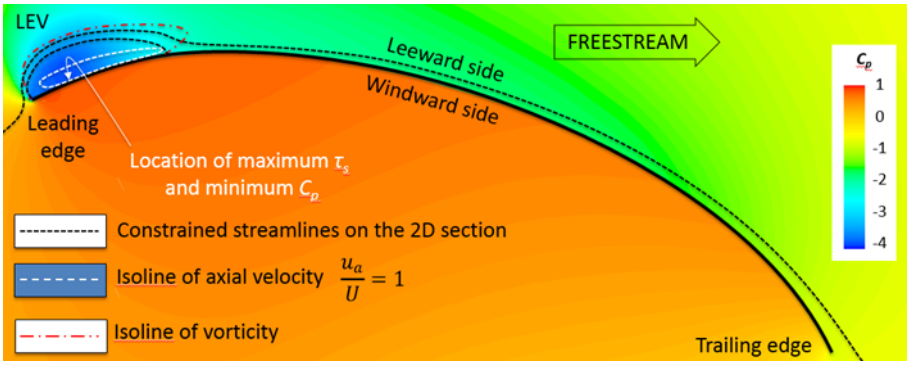

Figure 3: The LEV computed on a horizontal section of an asymmetric spinnaker. Unpublished results from the time-averaged DES simulations of Viola et al. (2014).

The LEV has been identified with a highly time resolved DES (Viola et al., 2014) at lower Reynolds numbers than at full scale. In the opinion of the authors, despite the continuous growth of the computational resources, it is still not possible to use more advanced turbulence models such as Large Eddy Simulations (LES). The grid and time resolution required to apply an LES model is significantly higher to that of DES, and is unachievable even by very large supercomputers. However, some under-resolved simulations have been performed with some degree of success both for upwind (Nava et al., 2017) and downwind (Nava et al., 2018) sails. Nava et al. (2017) undertook LES of upwind sails and flat plates, where the latter investigation is based on the low-Reynolds number experimental work of Crompton & Barrett (2000) that has often been used as a benchmark for low-camber sails (Collie, 2006; Collie et al., 2008). A key advantage of LES over RANS was originally shown by Sampaio et al. (2014) and confirmed by Nava et al. (2017) on upwind sails: the ability to predict the second recirculation bubble typical of long leading-edge bubbles. Modelling correctly this secondary bubble, which sits between the leading edge and the main bubble core, is critical to accurately predict the direction of the separated shear layer and thus the reattachment point of the bubble. Therefore, while the use of LES for yacht sails is expected to significantly improve the accuracy of the solution, the required computational power is still unaffordable.

5. LEADING-EDGE VORTEX OF DOWNWIND SAILS: EXPERIMENTAL MEASUREMENTS

Model-scale testing of a solid asymmetric spinnaker, similar to that of the previous numerical work (Viola et al., 2014), was conducted in the current flume at the University of Edinburgh, utilizing PIV to provide flow visualization. This experiment confirmed the existence of the LEV on the upper half of an asymmetric spinnaker. Vorticity formed at the leading edge rolls up and it is extracted by axial flow at the top of the sail, providing between 10% and 20% of the total sectional lift. It is suggested that the overall contribution to lift generation on the whole sail could be significantly more than 10% (Arredondo-Galeana & Viola, 2018).

The LEV was observed to be stable only intermittently (Figure 4a and 4b). When unstable, it was continuously formed and, once it reached a critical strength, convected downstream (Figure 4c). The aerodynamic forces depend on the position and velocity of the LEV with respect to the sail. Hence the convection of the LEV could lead to mild load fluctuations. However, the distance between two convecting LEVs is a fraction of the sail chord, and hence several LEVs are simultaneously present on the leeward side of the sails (Figure 4c). This mitigates the load fluctuations associated with the convection of each LEV. Moreover, the mean aerodynamic forces were similar for the stable and unstable mode of the LEV.

Figure 4a shows the experimental time averaged-streamlines of a section of the model spinnaker (Arredondo-Galeana & Viola, 2018) at 75% of the span from the foot. Figures 4b and 4c show a stable and a shedding LEV respectively, modelled through a potential flow approach, where the circulation and position of each vortex was informed by the PIV measurements. This modelling approach informed by the experiments allows the quantification of the contribution of the LEV to the sectional lift of the spinnaker.

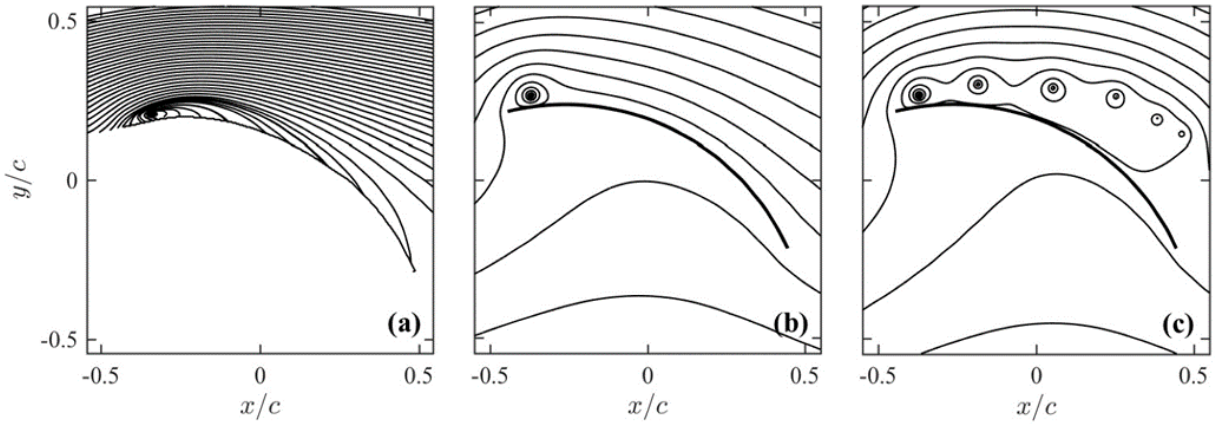

Figure 4: The LEV computed and modelled on a horizontal section of an asymmetric spinnaker. The experimental time-averaged streamlines (a) measured by Arredondo-Galeana & Viola (2018); the complex potential model of the LEV when steady (b) and when unsteady (c). The x and y axes are streamwise and orthogonal to the flow direction, respectively, centred at the mid-chord and normalised with the chord length c.

6. MODEL-SCALE / FULL-SCALE CORRELATION

6.1. Background on Full-Scale Testing

Despite the earliest report of full-scale testing on yacht sails dating back to 1923 (Marchaj, 1979), the absence of correlation between the measurements and sail shape has been a major limit in the study of sail aerodynamics. With the growing interest for numerical modelling, advances in sensors, full-scale testing and the validation of numerical simulations and model-scale tests, there is a strong demand for full-size benchmark cases.

With the development of dedicated wind tunnels in the 90s, the demand for validation data and benchmarks led to full-scale measurements to be performed on a 35-footer by Milgram et al. (1993). Subsequently, similar experiments were performed on 33-footers by Masuyama & Fukasawa (1997) and Hochkirch & Brandt (1999) respectively. The former primarily focused on sail forces for the purpose of velocity prediction, and achieved a good agreement between the experimental data gathered (on both tacks) and numerical methods such as vortex lattice and RANS CFD, based on the sail shapes recorded by on-board

cameras. This experiment primarily tackled upwind sails and the numerical validation with full-scale data.

Hansen et al. (2003) targeted downwind sails, with a validation focused on comparison between full-size and wind tunnel data. More recently, load and position sensors were fitted to the spinnaker of a 26-footer (J-80) by Augier et al. (2012), this time with a stronger emphasis on the more realistic unsteady fluid-structure interaction. Indeed, the greater availability of computer power now allows to run more cost-effective virtual wind tunnel tests with FSI, modelling the changes between the moulded and flying shape depending on the point of sail, wind speed and trim. An area where more research is certainly needed is, for example, luff flapping (Viola & Flay, 2009; Deparday, 2016; Aubin et al., 2018).

Full-scale pressure measurements have, in some instances, provided evidence of the presence of the LEV. Viola & Flay (2011) identified a suction peak at the trailing edge of full-scale downwind sails at high apparent wind angles. It is argued that this is evidence of delta wing-like vortex formation on the top section of the spinnaker.

Motta et al. (2015) also performed full-scale pressure measurement, detecting low pressure peaks convecting chordwise; a phenomenon assimilated to the shedding of an LEV. This is also the argument brought forward by Richards & Viola (2015): the inability to sustain an LEV leads to its shedding in the upper sections of asymmetric spinnakers. LEV shedding was, in fact, observed in the water channel experiments of Arredondo-Galeana & Viola (2018).

6.2. On Water, Wind Tunnel and Computational Measurements

Viola & Flay (2011) compared the forces and pressures measured at full-scale on water, at model-scale in the wind tunnel, and numerically using RANS. This was performed on both upwind and downwind sails, the latter being of primary interest in this instance. In this study, the drive and side force coefficients were shown to be within 0.5% between the wind tunnel and numerical models. However, significant differences were observed on the pressure distributions. Due to their free leading edge, spinnakers tend to be trimmed tighter in full-scale sailing conditions to prevent the luff from collapsing. Conversely, in the steadier conditions of the wind tunnel, the spinnaker can be eased closer to the flapping point. This is revealed in Figure 5, where the single suction peak for the full-scale spinnaker suggests that it is trimmed too tightly. Conversely, the wind tunnel and the numerical simulation feature two suction peaks, suggesting a lower angle of attack. Here the sails were trimmed for the maximum drive force.

It is interesting to observe that the RANS simulations of Viola & Flay (2011) already provided insights into the presence of a tri-dimensional LEV, but these could not be fully recognised because the simulations were not time-resolved. Hence, the helicoidal flow pattern in the region of separated flow near the leading edge was interpreted as a feature of the time-averaged LSB.

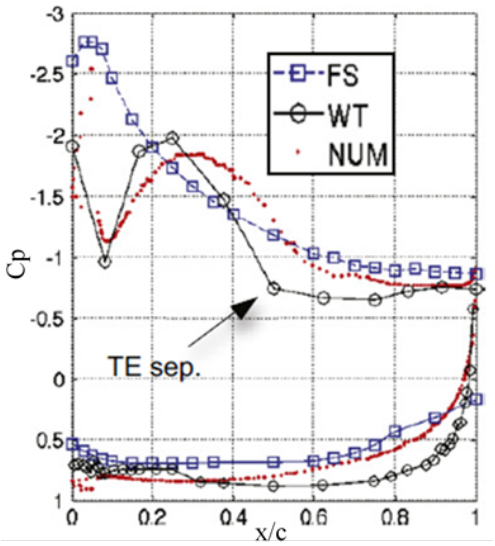

Figure 5: Pressure distributions on the mid-span section of an asymmetric spinnaker, measured at full-scale (FS), in a wind tunnel (WT) and computed numerically (NUM) by Viola & Flay (2011). The x axis is chordwise, from the leading edge and normalised with the chord length c.

7. LEADING-EDGE-SEPARATION BUBBLE AND LAMINAR-SEPARATION BUBBLE

As previously highlighted, when the LEV of downwind sails is unstable, it is shed downstream and convected along the surface of the sail (Richards & Viola, 2015), ultimately resulting in a similar time-averaged flow field to that of leading-edge bubbles. A similar phenomenon occurs on upwind fore sails, such as jibs and genoas.

Ota et al. (1981) showed that the flow regime of leading-edge separation bubbles can be equally laminar, transitional (i.e. laminar-to-turbulent transition occurs on the separated shear layer), or turbulent (with either turbulent separation, or transition immediately downstream of the separation point). The instantaneous vorticity field and the time-averaged velocity field of leading-edge bubbles can be found in Figures 2a and 2b respectively. The time averaged and instantaneous flow fields of an LSB, shown in Figure 2c, are similar to those of a leading-edge bubble. Following the separation of the boundary layer due to an adverse pressure gradient, a laminar to turbulent transition occurs, with a reattachment downstream, thus forming a laminar-separation bubble. The LSB can be identified thanks to the presence of a plateau in the pressure distribution (Ward, 1963). Increasing the Reynolds number and the background turbulence, the transition and reattachment points move upstream, hence the length of the bubble decreases (O'Meara & Mueller, 1987). Conversely, increasing the AoA, the separation point moves downstream and the length of the bubble increases.

In this paper, the term LSB is used differently from several other papers, including those of the very same authors. Here the LSB is used to identify a separation bubble where the key mechanisms of reattachment are due to the laminar to turbulent transition. In fact, one of the aims of this paper is to emphasise that the leading-edge bubble of model-scale sails may remain laminar. Consequently, the reattached boundary layer is laminar. In this case, the sail curvature may lead to separation of the laminar boundary layer, resulting in two possible outcomes: either an LSB is formed and hence the flow reattaches forming a turbulent boundary layer; or reattachment does not occur. It will be shown in the following section how these two outcomes leads to very different pressure distributions and lift forces.

The presence of the leading-edge bubble on yacht sails has been shown on model-scale downwind sails in wind tunnels (Viola & Flay, 2009), on circular arcs in CFD (Brault, 2013), and on circular arcs in wind tunnel (Flay, et al., 2017). These results are sometimes contradictory because of misinterpretations of the role of the vortex in generating lift, and in the assumption that it would have always triggered laminar-to-turbulent transition.

In some of these past experiments, the leading-edge bubble was laminar and the boundary layer downstream of the reattachment was also laminar. As noted by Flay et al. (2017), this observation is supported by evidence of an LSB farther downstream along the chord. For example, Martin (2015), Flay et al. (2017) and Nava et al. (2017) have shown a clear LSB towards the rear of a circular arc, especially for a low AoA (lesser than the ideal one), and low Reynolds number. The sudden change occurring below and above a specific critical Reynolds number was discussed by Flay et al. (2017).

For greater Reynolds numbers, the flow behaviour is closer to that of a streamlined profile. In these conditions, transitions occurs upstream of trailing edge separation, either within the leading-edge bubble or between the reattachment point and the LSB. Consequently, the boundary layer remains attached longer, decreasing both the wake and the drag, while the improved suction region results in higher lift, as is the case, for instance, of Nava et al. (2016). The LSB is also observed at angles of attack below the ideal one, where there is no leading-edge bubble.

These discrepancies motivated further work to be undertaken on a circular arc, which has the same camber of a typical spinnaker. It will be shown in the next section that a laminar leading-edge separation bubble may indeed occur on model scale sails, resulting in an unrealistic laminar trailing-edge separation. Importantly, the next section will describe the conditions at which model-scale sails must be tested to prevent this effect.

8. HIGHLY-CAMBERED, THIN, CIRCULAR ARC

8.1. Background

The use of a highly cambered (over 20% camber) thin circular arc with a sharp leading edge has been used extensively in recent years to further the understanding of the flow field past downwind sails. Indeed, the circular arc represents a typical cross section through a modern asymmetric spinnaker. The geometry was originally employed by Velychko (2014) in wind tunnel tests, followed by numerical work (Brault, 2013) and by water tunnel experiments (Lebret, 2013; Lombardi, 2014; Martin, 2015; Thomas, 2015; Couvrant, 2015). These research works, together with other wind tunnel tests on the same geometry, are reported by Flay et al. (2016).

From these results, it was unclear which was the minimum AoA at which the leading-edge bubble occurs (i.e. the ideal angle of attack), and if the appearance of the bubble resulted in a lift increase or decrease. It was also unclear if, and where, laminar-to-turbulent transition occurred and its effect on the lift.

8.2. Method

To investigate, a carbon fibre circular arc was built, with a chord of 200 mm and a camber of 22.32% (as per the literature). Pre-preg was employed to achieve the thinnest possible

geometry, more representative of the thin membrane than spinnakers are. The final thickness of the tested arc was 1.8 mm.

The force measurements were recorded at 1000 Hz for 6 seconds, at speeds equivalent to Re found in the literature, namely 53k, 68k, 150k and 220k. This allowed to validate the accuracy of the forces measured against Velychko (2014) and demonstrated an abrupt increase in lift and decrease in drag at a critical AoA for a given Re. Additional work on flow visualisation was then carried out using PIV on the same geometry, in order to provide a physical explanation to the abrupt change in lift coefficient. Transition was detected by quantifying the Turbulent Kinetic Energy (TKE) from one hundred pairs of PIV flow fields.

8.3 Results

The experiments reveal that, at low Re, the leading-edge bubble is laminar! This demonstrates that at model scale there might be a non-realistic laminar boundary layer, which is more prone to separation than the turbulent boundary layer at full scale. These experiments showed there is an AoA at which the reattached, laminar, boundary layer turns into turbulent before trailing edge separation occurs. The authors called this angle the 'critical AoA'. In order to correctly scale the point where trailing-edge separation occurs on a scaled model, tests must be performed at an AoA higher than this angle. This angle decreases with the Re.

Figure 6a shows a sub critical AoA, where trailing-edge separation is laminar and transition occurs in the separated shear layer. Conversely, Figure 6b shows a super-critical AoA, where transition occurs in the boundary layer and trailing-edge separation is turbulent. The turbulent boundary layer is more resilient to separation and, hence, trailing edge separation occurs further downstream.

In order to investigate the effect of the leading-edge bubble on the lift force, the minimum AoA at which the bubble occurs is investigated. Figure 7 highlights the position of the stagnation point near the leading edge (LE) of the arc for different AoA. This figure clearly reveals that 11 degrees (deg) is the ideal AoA for the tested circular arc: the leading-edge bubble must occur at 11 deg and cannot occur at 10 deg.

Wind tunnel tests of flexible sails are performed only at AoA higher than the ideal AoA. Hence, the Re at which the critical AoA is 11 deg was searched for. The authors called this Reynolds number the 'critical Re'. If a circular arc is tested at the critical Re or higher, there is no risk of laminar trailing-edge separation. It was ascertained that, for the tested model, the critical Re is 144k (±2k). It must be remarked that the critical Re and the critical AoA depend on the specific geometry.

Finally, by combining the existing literature data (Lombardi, 2014; Velychko, 2014) and devised experiments, a schematic diagram of how the lift coefficient varies with the AoA was produced, as depicted in Figure 8. A low lift coefficient curve corresponds to subcritical AoA and Re. Past a Re of 218k, the flow will be turbulent for any AoA. However, for each lower Re, there is a critical AoA, where the lift abruptly increases due to the transition in the boundary layer.

8.4 Discussion

The recent research findings inherent to the highly cambered thin circular arc with sharp leading edge yielded four significant results. Firstly, there is a combination of critical AoA and critical Re that define when the laminar to turbulent transition occurs upstream of the trailing-edge separation point, resulting in higher lift and lower drag. On the other hand, for the critical Re ≈ 220k, this occurs for any AoA. At the critical Re = 68k, the critical AoA is between 14 deg and 15 deg, which is consistent with previous work (Lombardi, 2014).

The leading-edge bubble is not correlated with the discontinuous lift jump, which instead is due to the transition in the boundary layer. For example, Martin (2015) speculated that the growth of the leading-edge bubble was causing the jump in lift. However, the present work shows that this is not the case, and the previous conclusion drawn were a coincidence of the tested Re.

Thirdly, the ideal AoA for the circular arc, previously defined as 8 deg by Martin (2015) based on the peak in lift coefficient has been shown to be erroneous. Indeed, PIV revealed that the stagnation point was located on the leading edge at an AoA of 11 deg This is consistent with the PIV measurements of Thomas (2015).

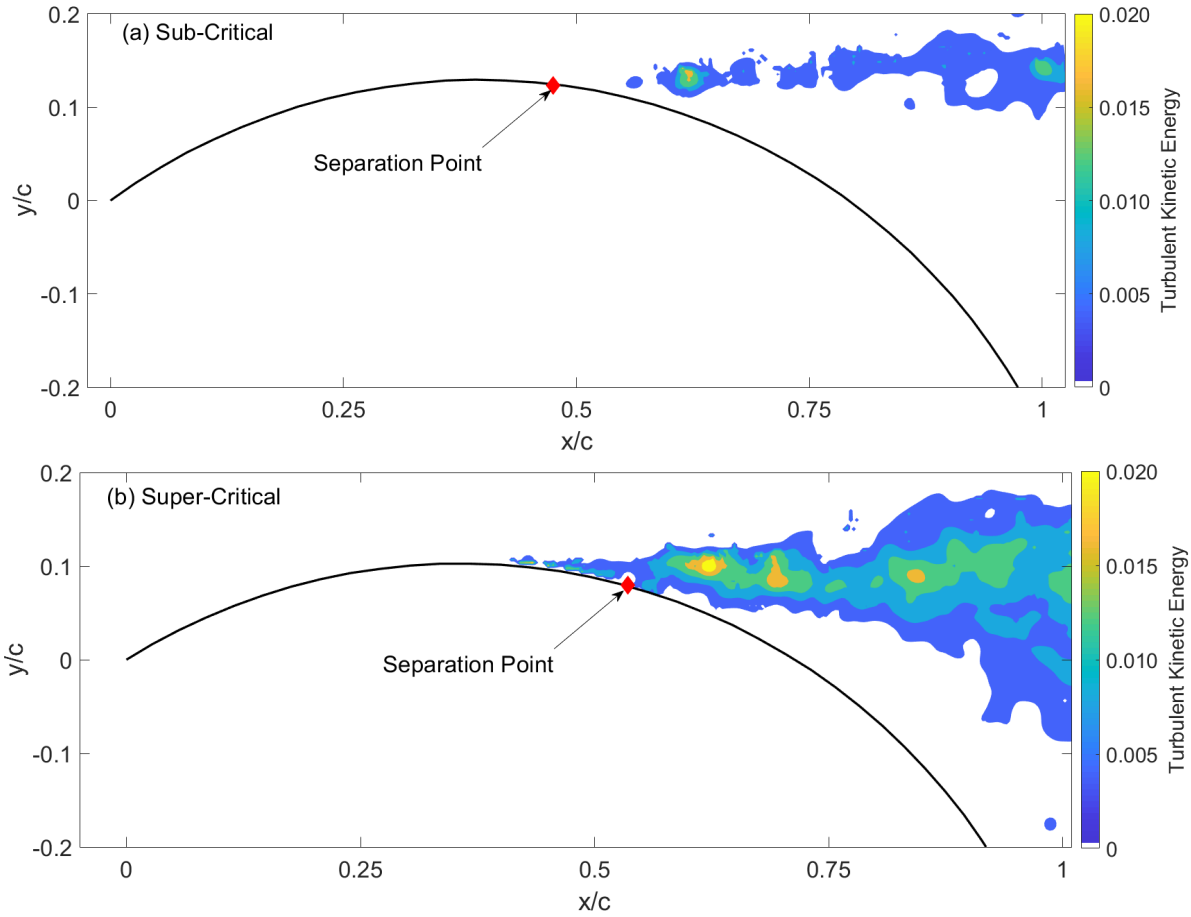

Figure 6: Flow measurements over a circular arc. Contours of turbulent kinetic energy, and position of the separation point over a circular arc at Re = 68k and at: a) sub-critical AoA and b) super-critical AoA. The x and y axes are streamwise and orthogonal to the flow direction, respectively, centred at the leading edge and normalised with the chord length c.

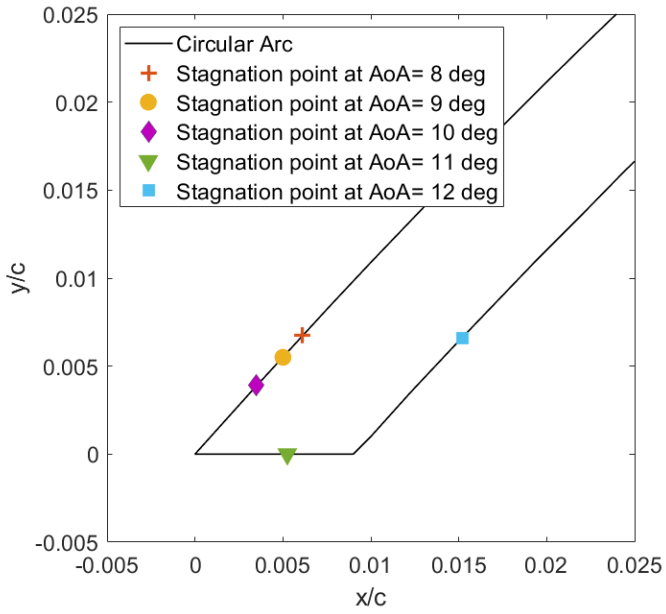

Figure 7: Location of the stagnation point at the leading edge of a highly cambered, thin circular arc for different AoAs. The x and y axes are chordwise and orthogonal to the chord, respectively, centred at the leading edge and normalised with the chord length c.

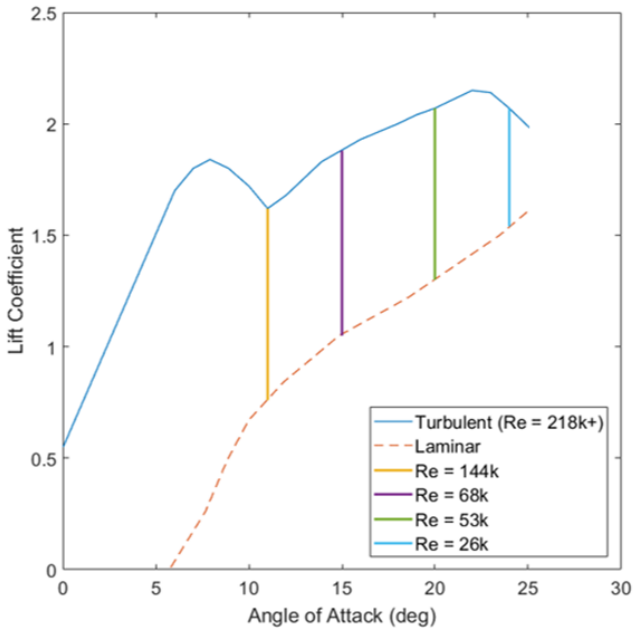

Figure 8: Schematic diagram of the lift curve and critical AoAs for different Re.

Lastly, the present results show that, for this model, the critical Re = 144k (±2k) is associated with a critical AoA that coincides with the ideal AoA, 11 deg. Let assume, in first approximation, that this is the critical Re of the ideal AoA also for a model-scale sails. For Re higher than 144k (±2k), transition would occur upstream of trailing-edge separation, as on a full-scale sail.

These results suggest that, for a highly cambered model-scale sail, Re should be much higher than 144k (±2k) so that the model flow field is as per the full-size. It should be reminded that this limiting Re is likely to strongly depend on the sail curvature, and probably on the twist, the background turbulence and surface roughness. For example, the tests by Bot et al. (2014) on a rigid model-scale sail suggest that Re = 230k was insufficient for their model. In fact, reviewing their sail pressure distributions in light of these findings, the presence of the LSB can clearly be identified (Figure 9). Bot et al. (2014) tested at an average chord-based Re of 230k. This represents an example of a test where too low a Re was employed, with the critical AoA occurring after the ideal AoA.

Similarly, circular arcs at low Re have showcased an LSB, the evidence of which was provided either numerically with the average velocity field (Brault, 2013), or experimentally with pressure taps (Flay et al., 2017). The latter also reported both an AoA and Re dependency. Conversely, no evidence of an LSB can be found in the literature for full size spinnakers, including the experiments reported by Viola and Flay (2011), Motta et al. (2014) and Deparday et al. (2017).

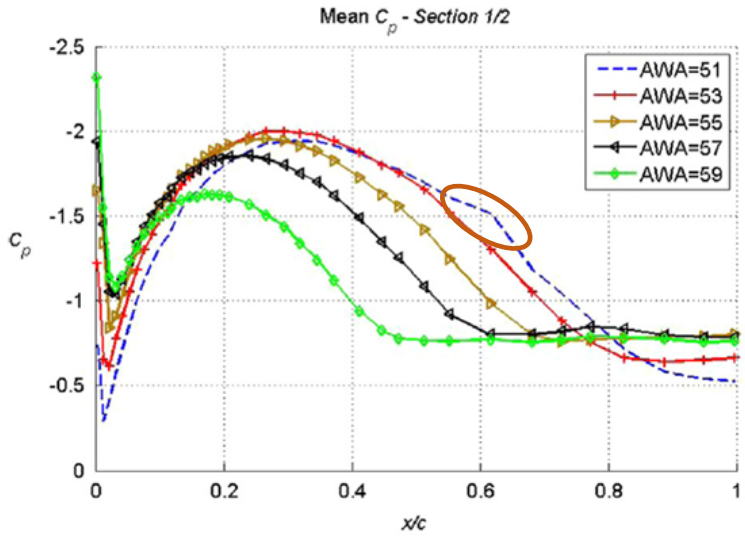

Figure 9: Pressure coefficient along the mid-section of a spinnaker (Bot et al., 2014). The x axis is chordwise, from the leading edge and normalised with the chord length c.

9. CONCLUSIONS

In the last decade, significant progress has been made on the understanding of the aerodynamics of sails, and particularly on flow at the leading edge and laminar-to-turbulent transition in the boundary layer. The leading-edge vortex was first shown to be present on spinnakers in 2014 numerically and confirmed experimentally in 2017. Nonetheless, more research is needed to confirm that the LEV actually exists in a coherent structure at full-scale and in a realistic unsteady flow condition, which are the sail types and apparent wind angles at which it occurs, and how it can be exploited by design.

The last decade also saw significant advances in the correlation between the surface pressure distributions measured in wind tunnel, computed numerically or measured on full-scale sails. This now leads to a better understanding of the flow features affecting the design and testing of asymmetric spinnakers. Anomalies in some pressure distributions measured at model scale prompted further work to be conducted on highly cambered thin circular arcs resembling a 2D section of an asymmetric spinnaker. In this paper, some new key results of this model are presented. These experiments demonstrated that several wind tunnel tests were performed at too low Reynolds numbers. At the low Reynolds numbers, the leading-edge bubble is laminar, and hence the reattached boundary layer is laminar, and trailing edge separation might occur upstream of where a turbulent boundary layer would have separated. Transition was shown to be governed by the combination of a critical Reynolds number and a critical AoA. The analysis of previous work in light of these new results suggests that model-scale tests should conservatively be tested at Re > 230k.

These results further supported recent findings on the importance of the leading-edge vortex in lift generation. Indeed, noting the recent experimental evidence suggesting that up to 20% of the sectional lift can be provided by the LEV, it is envisaged that future work will see a stronger emphasis on how to promote a sustainable leading-edge vortex by design. Moreover, the leading-edge vortex being located at the luff of the sail, the relative increase in driving force will be substantially higher than the increase in lift. Hence, downwind sail design, and more precisely modern asymmetric spinnakers, can be tremendously refined by fully exploiting the effect of the LEV as part of the sail design process.

10. REFERENCES

Arredondo-Galeana, A. (2019). *A study of the vortex flows of downwind sails*. PhD Thesis, University of Edinburgh, UK.

Arredondo-Galeana, A. & Viola, I.M. (2018). The leading-edge vortex of yacht sails. *Ocean Engineering*, vol. 159, pp. 552-562.

Aubin, N., Augier, B., Deparday, J., Sacher, M., & Bot, P. (2018). Performance enhancement of downwind sails due to leading edge flapping: A wind tunnel investigation. *Ocean Engineering*, 169, 370-378.

Augier, B., Bot, P., Hauville, F., & Durand, M. (2012). Experimental validation of unsteady models for fluid structure interaction: application to yacht sails and rigs. *Journal of Wind Engineering and Industrial Aerodynamics,* vol. 101, pp. 53-66.

Bethwaite, F. (1993). *High performance sailing*. International Marine Publication Company.

Bomphrey, R.J., Lawson, N.J., Harding, N.J., Taylor, G.K. & Thomas, A.L.R. (2005). The aerodynamics of Manduca sexta: digital particle image velocimetry analysis of the leading-edge vortex. *The Journal of Experimental Biology*, vol. 208, pp. 1097-1094.

Borazjani, I. & Daghooghi, M. (2013). The fish tail motion forms an attached leading edge vortex. *Biological Sciences*, The Royal Society, vol. 280, pp. 2012-2071.

Bot, P., Viola, I.M. & Flay, R.G.J., & Brett J.S. (2014) Wind-tunnel pressure measurements on model-scale rigid downwind sails. *Ocean Engineering*, vol. 90, pp. 84-92.

Brault, E. (2013). *Aerodynamics of Very Thin Airfoil*. Newcastle: MSc Thesis, Newcastle University.

Carter, R. (2006). Boat remains and maritime trade in the Persian Gulf during the sixth and fifth millennia BC. *Antiquity*, vol. 80(307), pp. 52-63.

Collie, S. (2006). *Application of computational fluid dynamics to two-dimensional downwind sail flows*. Auckland: PhD thesis, The University of Auckland.

Collie, S., Gerritsen, M., Jackson, P. (2008). Performance of Two-Equation Turbulence Models for Flat Plate Flows with Leading Edge Bubbles. *Journal of Fluid Engineering – Transactions of ASME*, vol. 130, issue 2.

Corke, T.C. & Thomas, F.O. (2015). Dynamic stall in pitching airfoils: aerodynamic damping and compressibility effects. *Annual Reviews in Fluid Mechanics*, vol. 47, pp. 479–505.

Couvrant, H. (2015). *Reynolds number and angle of attack effects on a leading edge vortex (LEV) for a highly cambered thin profile*. Brest: IERNAV.

Crabtree, L. F. (1977). *The formation of regions of separated flow on wing surfaces*. Aeronautical research council reports and memoranda.

Crompton, M. & Barrett, R. (2000). *Investigation of the separation bubble formed behind the sharp leading edge of a flat plate at incidence*. Proceedings of the Institution of Mechanical Engineers, Part G, vol. 214, pp. 157-176.

Deparday, J. (2016). *Experimental studies of fluid-structure interaction on downwind sails*. Brest: PhD thesis, Universite de Bretagne Occidental.

Deparday, J., Bot, P., Hauville, F., Augier, B. & Rabaud, M. (2017). Modal Analysis of Pressures on a Full-Scale Spinnaker. *Journal of Sailing Technology*.

DeVoria, A.C., & Mohseni, K. (2017). On the mechanism of high-incidence lift generation for steadily translating low-aspect-ratio wings. *Journal of Fluid Mechanics*, vol. 813, pp. 110-126.

Durand, M., Leroyer, A., Lothodé, C., Hauville F., Visonneau, M., Floch, R. & Guillaume, L. (2014). FSI investigation on stability of downwind sails with an automatic dynamic trimming. *Ocean Engineering*, vol. 90, pp. 129-139.

Earnshaw, P.B. (1962). *An experimental investigation of the structure of a leading-edge vortex.* Aeronautical Research Council Reports and Memoranda.

Eldredge, J.D. & Jones, A.R. (2019). Leading-Edge Vortices: Mechanics and Modelling. *Annual Reviews of Fluid Mechanics*, vol. 51, pp. 75–104.

Ellington, C., van den Berg, C., Willmott, A. & Thomas, A. (1996). Leading-edge vortices in insect flight. *Nature*, vol. 384, pp. 626-630.

Fallow, B.J. (1996). America's Cup sail design. *Journal of Wind Engineering and Industrial Aerodynamics*, vol. 63, pp. 183-192.

Flay, R.G.J. & Jackson, P. S. (1992). Flow simulation for wind tunnel Studies of sail aerodynamics. *Journal of Wind Engineering and Industrial Aerodynamics*, vol. 41-44, pp. 2703-2714.

Flay, R.G.J., Piard, A. & Bot, P. (2017). *Aerodynamics of a highly cambered circular arc aerofoil: experimental investigations*. International Conference on Innovation in High Performance Sailing Yachts, Lorient, France, pp.150-162.

Flay, R.G.J. & Vuletich, I.J. (1995). Development of a wind tunnel test facility for yacht aerodynamic studies. *Journal of Wind Engineering and Industrial Aerodynamics*, vol. 58, pp. 231-258.

Fossati, F. (2009). *Aero-Hydrodynamics and the Performance of Sailing Yachts*. London: Adlard Coles Nautical.

Gentry, A. (1971). *The aerodynamics of sail interaction*. The Ancient Interface III, 3rd AIAA Symposium on Sailing, Redondo Beach, California, US.

Gentry, A. (1988) *The application of computational fluid dynamics to sails*. Newport, Rhode Island, Proceedings of the Symposium of Hydrodynamic Performance Enhancement for Marine Applications.

Gursul, I., Gordnier, R., Visbal, M. (2005). Unsteady aerodynamics of nonslender delta wings. *Progress in Aerospace Sciences*, vol. 41, pp. 515–557.

Gursul, I.,Wang, Z. & Vardaki, E. (2007). Review of flow control mechanisms of leading-edge vortices. *Progress in Aerospace Sciences*, vol. 43, pp. 246–270.

Hall, M. (1961). A theory for the core of a leading-edge vortex, Journal of Fluid Mechanics, vol. 209, pp. 209-228.

Hansen, H., Jackson, P.S. & Hochkirch, K. (2003). Comparison of wind tunnel and full-scale aerodynamic sail force measurements. *International Journal of Small Craft Technology*, RINA Transactions, vol. 145(B1), pp. 23-31.

Harvey, J. (1959). *Some measurements on a yawed slender delta wing with leading edge separation*. A.R.C. R.&M. 3160.

Hedges, K.L. (1993). *Computer modelling of downwind sails*. ME Thesis, University of Auckland, New Zealand.

Hedges, K., Richards, P. & Mallison, G. (1996). Computer modelling of downwind sails. *Journal of Wind Engineering and Industrial Aerodynamics*, vol. 63, pp. 95-110.

Hochkirch, K. & Brandt, H. (1999). Full-scale hydrodynamic force measurement on the berlin sailing dynamometer, Proceedings of the 14th Chesapeake Sailing Yacht Symposium, January 30th, Annapolis, MD, pp. 33-44.

Huang, M.K. & Chow, C.Y. (1982). Trapping of a free vortex by Joukowski airfoils. *AIAA Journal,* vol. 20, pp. 292–298.

Hubel, T.Y. & Tropea, C. (2010). The importance of leading edge vortices under simplified flapping flight conditions at the size scale of birds. *Journal of Experimental Biology*, vol. 213, pp. 1930–1939.

King, R. (1981). *Spinnaker*. London: Granada Publishing.

Larsen, J.W., Nielsen, S.R.K. & Krenk, S. (2007). Dynamic stall model for wind turbine airfoils. *Journal of Fluids and Structures*, vol. 23, pp. 959–982.

Larsson, L., Eliasson, R.E. & Orych, M. (2013). *Principles of Yacht Design*. International Marine Publishing Co, 4th edition.

Lasher, W.C., Sonnenmeier, J.R., Forsman, D.R. & Tomcho, J. (2005). The aerodynamics of symmetric spinnakers. *Journal of Wind Engineering and Industrial Aerodynamics*, vol. 93, pp. 311-337.

Lebret, C. (2013). *High Cambered thin profile study*. Auckland: The University of Auckland.

Lentink, D., Dickson, W.B., van Leeuwen, J.L., Dickinson, M.H. (2009). Leading-edge vortices elevate lift of autorotating plant seeds. *Science,* vol. 324, pp. 1438–1440.

Lentink, D., Müller, U.K., Stamhuis, E.J., de Kat, R., van Gestel, W., Veldhuis, L.L.M., Henningsson, P., Hedenström, A., Videler, J.J. & van Leeuwen, J.L. (2007). How swifts control their glide performance with morphing wings. *Nature*, vol. 446, pp. 1082–1085.

Li, J. & Wu, Z.N. (2018). Vortex force map method for viscous flows of general airfoils. *Journal of Fluid Mechanics*, vol. 836, pp. 145-166.

Lombardi, A. (2014). *Experimental analysis of a highly-cambered thin profile*. Strathclyde: MSc Thesis, University of Strathclyde.

Marchaj, C. (1979). *Aero-hydrodynamics of sailing*. Dodd Mead and Company, New York.

Marsden, D., Simpson, R. & Rainbird, W. (1958). *An investigation into the flow over delta wings at low speeds with leading edge separation*. Cranfield: College of Aeronautics, Cranfield Report No. 114. ARC 20,409.

Martin, V. (2015). *Reynolds number and angle of attack effects on a highly cambered thin profile flow topology*. Brest: IRENAV Laboratory.

Masuyama, Y. & Fukasawa, T. (1997). *Full-Scale Measurements of Sail force and Validation of Numerical Calculation Method.* Proceedings of the 13th Chesapeake Sailing Yacht Symposium, January 25th, Annapolis, MD, pp. 23-36.

Mcauliffe, B.R. & Yaras, M. (2010). Transition mechanisms in separation bubbles under low and elevated-freestream turbulence. *Journal of Turbomachinery*, vol. 132 (1).

Milgram, J.H. (1968). *The Aerodynamic of sails*. Proceedings of the 7th Symposium on Naval Hydrodynamic, pp. 1397-1434.

Milgram, J.H., Peters, D.B. & Eckhouse, D.N. (1993). *Modelling IACC sail forces by combining measurements with CFD*. Proceedings of the 11th Chesapeake Sailing Yacht Symposium, January 29th-30th, Annapolis, MD, pp. 65-73.

Mitchel, A.M., Morton, S. A., Forsythe, J.R. & Cummings, R.M. (2006). Analysis of delta-wind vortical substructures using detached-eddy simulation. *AIAA Journal*, vol. 44 (5), pp. 964-972.

Miyata, H. & Lee, Y. (1999). Application of CFD simulation to the design of sails. *Journal of Marine Science and Technology*, vol. 4, pp. 163-172.

Motta, D., Flay, R.G.J., Richards, P.J., Le Pelley, D.J. & Deparday, J. (2014). Experimental Investigation of Asymmetric Spinnaker Aerodynamics Using Pressure and Sail Shape Measurements. *Ocean Engineering*, vol. 90, pp. 104-118.

Motta, D., Flay, R.G.J., Richards, P.J., Le Pelley, D.J., Bot, P. & Deparday, J. (2015). *An investigation of the dynamic behaviour of asymmetric spinnakers at full-scale*. 5th High Performance Yacht Design Conference, Auckland, New Zealand.

Muijres, F.T., Johansson, L.C., Barfield, R., Wolf, M., Spedding, G.R. & Hedenström, A. (2008). Leading-edge vortex improves lift in slow-flying bats. *Science*, vol. 319, pp. 1250–1253.

Nava, S., Bot, P. & Carter, J. (2006). *Modelling the lift crisis of a cambered plate a 0 degrees angle of attack.* 20th Australasian Fluid Mechanics Conference, Perth, Australia.

Nava, S., Cater, J. & Norris, S. (2017). Modelling leading edge separation on a flat plate and yacht sails using LES. *International Journal of Heat and Fluid Flow*, vol. 65, pp. 299-308.

Nava, S., Cater, J. & Norris, S. (2018). Large Eddy Simulation of an asymmetric spinnaker. *Ocean Engineering*, vol. 169, pp. 99-109.

Newman, B.G. & Tse, M.C. (1992). Incompressible flow past a flat plate aerofoil with leading edge separation bubble. *Aeronautical Journal*, vol. 96, pp. 57-64.

O'Meara, M.M. & Mueller, J.T. (1987). Laminar separation bubble characteristics on an airfoil at low Reynolds numbers. *AIAA Journal*, vol. 25(8), pp. 1033-1041.

Ota, T., Asano, Y. & Okawa, J.I. (1981). *Reattachment length and transition of the separated flow over blunt flat plates*. Bulletin of the JSME, vol. 24(192), pp. 941-947.

Polhamus, E.C. (1966). *A concept of the vortex lift of sharp-edge delta wings based on a leading-edge suction analogy*. NASA Technical Report TND-3767.

Renzsch, H., Muller, O. & Graf, K. (2008). *FLEXSAIL – a fluid structure interaction program for the investigation of spinnakers*. Proceedings of the International Conference on Innovations in High Performance Sailing Yachts, Lorient, France.

Richards, P.J., Johnson, A. & Stanton A. (2001). America's Cup sails – vertical wings or horizontal parachutes? *Journal of Wind Engineering and Industrial Aerodynamics*, vol 89, pp 1565-1577.

Richards, P.J. & Viola, I.M. (2015). *Leading Edge Vortex Dynamics*. 17th Australian Wind Engineering Society Workshop, Wellington, New Zealand.

Richter, H.J., Horrigan, K.C. & Braun, J.B. (2003). Computational fluid dynamics for downwind sails. Proceedings of the 16th Chesapeake Sailing Yacht Symposium, Annapolis, Maryland, USA.

Sacher, M., Hauville, F., Bot, P. & Durand, M. (2015). *Sail trimming FSI simulation - comparison of viscous and inviscid flow models to optimise upwind sails trim*. 5th High Performance Yacht Design Conference, HPYD 2015, pp. 217-228, Auckland, New Zealand.

Saffman, P.G. & Sheffield, J.S. (1977). Flow over a Wing with an Attached Free Vortex. *Studies in Applied Mathematics*, vol. 57, pp. 107–117.

Sampaio, L.E.B., Rezende, A.L.T., & Nieckele, A.O. (2014). The challenging case of the turbulent flow around a thin plate wind deflector, and its numerical prediction by LES and RANSE models. *Journal of Wind Engineering and Industrial Aerodynamics*, vol. 133, 52-64.

Stevenson, J.P.J., Nolan, K.P., & Walsh E.J. (2016). Particle image velocimetry measurements of induced separation at the leading edge of a plate. *Journal of Fluid Mechanics*, vol. 184, pp. 278-297.

Taira, K. & Colonius, T. (2009). Three-dimensional flows around low-aspect-ratio flat-plate wings at low Reynolds numbers. *Journal of Fluid Mechanics*, vol. 623, pp. 187-207.

Thomas, G. (2015). *Flow phenomenology around a highly cambered thin profile*. Brest: IRENAV.

Velychko, N. (2014). *Study of highly cambered aero foil using JR3 sensor*. Auckland: The University of Auckland.

Videler, J., Stamhuis, E. & Gde, P. (2004). Leading-edge vortex lift swifts. *Science*, vol. 306, pp. 1960-1962.

Viola, I.M. (2009). Downwind sail aerodynamics: a CFD investigation with high grid resolution. *Ocean Engineering*, vol. 36, pp. 974-987.

Viola, I.M. & Arredondo-Galeana, A. (2017). *The leading-edge vortex of yacht sails*. Innovsail International Conference on Innovation in High Performance Sailing Yachts, Lorient, France, pp. 115-126.

Viola, I.M., Bertesaghi, S., Van-Renterghem, T. & Ponzini, R. (2014). Detached eddy simulation of a sailing yacht. *Ocean Engineering*, vol. 90, pp. 93-103.

Viola, I.M. & Flay, R.G.J. (2009). Force and pressure investigation of modern asymmetric spinnakers. *International Journal of Small Craft Technology*, RINA Transactions, vol. 151 (B2).

Viola, I.M. & Flay, R.G.J. (2011). Sail pressures from full-scale, wind tunnel and numerical investigations. *Ocean Engineering*, vol. 38(16), pp. 1733-1743.

Viola, I.M. & Flay, R.G.J. (2012). Sail aerodynamics: on-water pressure measurements on a downwind sail. *Journal of Ship Research*, vol. 56 (4), pp. 197-206.

Viola, I.M. & Ponzini, R. (2011). *A CFD investigation with high-resolution grids of downwind sail aerodynamics.* International Conference on Developments in Marine CFD, London, UK.

Ward, J.W. (1963). The behaviour and effects of laminar separation bubbles on aerofoils in incompressible flow. *Journal of the Royal Aeronautical Society*, vol. 67, pp. 783-790.